



Density functional perturbation theory calculations of vibrational and thermodynamic properties of $Zn_{1-x}Be_xO$ alloys.



Said Lakel^{a,b,*}, Fatima Elhamra^a, K. Almi^b, H. Meradji^c

^a Laboratory of physical materials – University of Laghouat, BP 37G, Laghouat, Algeria

^b Laboratoire de Matériaux Semi Conducteurs et Métalliques «LMSM», Université de Biskra, Algeria

^c Laboratoire de Physique des Rayonnements, Université Badji Mokhtar Annaba, Algeria

ARTICLE INFO

Article history:

Received 12 March 2015

Received in revised form

1 May 2015

Accepted 19 May 2015

Keywords:

$Zn_{1-x}Be_xO$

DFT

DFPT

Lattice dynamics

Thermodynamic properties

Debye temperature

Heat capacity

ABSTRACT

The elastic, phonon and thermodynamic properties of $Zn_{1-x}Be_xO$ alloy are investigated by performing density functional theory (DFT) and density functional perturbation theory (DFPT) calculations. The calculated lattice parameters decreases with the increase of Be content that is in good agreement with the available theoretical and experimental data. The effect of Be composition on elastic constants was investigated for $Zn_{1-x}Be_xO$ alloys. Phonon dispersion curves show that $Zn_{1-x}Be_xO$ are dynamically stable. Thermodynamic properties, including Helmholtz free energy, enthalpy, entropy and heat capacity, were evaluated under quasi-harmonic approximation using the calculated phonon density of states. Finally, the results show that $Zn_{1-x}Be_xO$ alloys with lower Be content are more thermodynamically stable. The agreement between the present results and the known data that are available only for ZnO and BeO is generally satisfactory.

© 2015 Elsevier Ltd. All rights reserved.

1. Introduction

Zinc oxide (ZnO) is an attractive metal oxide because of its applicability for blue and ultraviolet (UV) light emitting diodes (LED) and laser diodes (LD) [1,2]. This interest stems from the electronic properties including a large direct band gap ($E_g=3.37$ eV at 300 K), a large exciton binding energy (~ 60 meV), strong spontaneous ($P_S=-0.57$ C/m²) and piezoelectric ($e_{33}=1.20$ C/m², $e_{31}=-0.56$ C/m²) polarizations, as well as the relative ease of synthesis of ZnO powders, single crystals, thin films, and nanostructures [3,4]. Due to these properties, ZnO is a key enabling material in sensors and actuators, transparent thin-film electronics, and optoelectronic and piezoelectric devices [5,6]. Furthermore, its low

material cost, high crystalline quality, and high radiation resistance make it a promising material to compete with GaN-based technologies [7].

Since reliable and stable p-type ZnO semiconductor material can now be grown using arsenic as dopant [8], a critical step for producing high-efficiency ZnO devices is the fabrication of ZnO-based quantum wells and superlattices. Since the electronic properties of ZnO can be readily tuned by doping or alloying, it is possible to expand its applications by designing materials systems for specific conditions and/or restrictions. For example, doping ZnO with Al (1–2%) or Ga (2–7%) results in a solid solution with a high carrier concentration ($\sim 10^{21}$ cm⁻³) and a commensurate low electric resistivity ($\sim 10^{-5}$ Ω cm) [9,10]. Such materials have already been incorporated in flat panel displays and solar cells as transparent electrodes to replace the relatively expensive In-Sn oxide (ITO) [11].

ZnO-based multiple quantum well structures such as ultra thin ZnO/ $Zn_{1-x}Mg_xO$ multi layers may provide better

* Corresponding author at: Laboratory of Metallic and Semiconducting Materials ♦ University of Biskra, B.P. 145 Biskra, Algeria. Tel.: + 213 0771409403.

E-mail address: s.lakel@yahoo.fr (S. Lakel).

Table 1Calculated lattice constants a and c of $Zn_{1-x}Be_xO$ after geometric optimization compared with available theoretical and experimental data.

x	a (Å)	a (Å)			c (Å)		
		This work	Expt.	Other calculations	This work	Expt.	Other calculations
$Zn_{1-x}Be_xO$	0	3.275	3.258 ^a	3.283 ^b , 3.256 ^c	5.304	5.220 ^a	5.309 ^b , 5.256 ^c
	0.25	3.145		3.134 ^c	5.132		5.076 ^c
	0.5	2.915		2.972 ^c	4.970		4.99 ^c
	0.75	2.788		2.889 ^c	4.528		4.675 ^c
	1	2.714	2.698 ^d	2.764 ^c	4.412	4.377 ^d	4.487 ^c

^a Ref. [31].^b Ref. [32].^c Ref. [33].^d Ref. [15].**Table 2**The calculated elastic constants for $Be_xZn_{1-x}O$ compared with both theoretical and experimental data.

		C_{11} (GPa)	C_{12} (GPa)	C_{13} (GPa)	C_{33} (GPa)	C_{44} (GPa)
ZnO	This work	209.52	127.65	117.50	213.00	42.95
	Experiments	206.217 ^a	118.117 ^a	118 ^a	211 ^a	44.50 ^a
	Calculations	227 ^b ; 217 ^c	55 ^b ; 117 ^c	93 ^b ; 121 ^c	206 ^b ; 225 ^c	49 ^b ; 50 ^c
		215.7 ^d ; 191.16 ^e	136.1 ^d ; 111.96 ^e	122.7 ^d ; 85.63 ^e	249.6 ^d ; 190.57 ^e	38.6 ^d ; 36.89 ^e
$Zn_{0.75}Be_{0.25}O$	This work	225.12	127.11	115.3	282.33	51.66
$Zn_{0.5}Be_{0.5}O$	This work	243.20	126.28	108.61	353.18	72.08
$Zn_{0.25}Be_{0.75}O$	This work	324.17	126.05	104.38	399.31	89.34
BeO	This work	462.55	124.55	83.58	495.39	135.70
	Experiments	460.6 ^f	126.5 ^f	88.5 ^f	491.6 ^f	147.7 ^f
	Calculations	432.5 ^d	135.8 ^d	99.0 ^d	474.1 ^d	131.3 ^d

^a Ref. [37].^b Ref. [38].^c Ref. [39].^d Ref. [40].^e Ref. [41].^f Ref. [42].

oscillation strength and enhanced exciton binding energy in blue and ultraviolet (UV) light emitting devices [12]. However, if ZnO-based solid solutions could be developed, they would work in this range; this would significantly reduce cost since ZnO is compatible with integrated circuit (IC) and can be synthesized with good stoichiometric control via a number of deposition methods [13].

Band-gap engineering of ZnO can be achieved by alloying with MgO ($E_g=7.70$ eV) for UV applications and such alloy can also be used as barrier layers in ZnO/(Zn,Mg)O superlattices for quantum well devices [14,15]. However, the phase separation occurs in $Zn_{1-x}Mg_xO$ solid solutions when the Mg composition exceeds 33% [15]. This is due to the differences in the crystal structures of ZnO [wurtzite, $P63mc$] and MgO (cubic, rocksalt). As such, the UV absorption range is limited to 3.37–3.90 eV in the $Zn_{1-x}Mg_xO$ system for $x < 0.33$ [16].

Therefore BeO ($E_g=10.60$ eV) which also crystallizes in the wurtzite structure has been considered as an alloying system of ZnO for UV optoelectronic devices and sensors. It was shown that $Zn_{1-x}Be_xO$ thin films can be deposited using hybrid beam deposition [17] with no phase separation over the entire composition range [15]. Furthermore, as the band gap in $Zn_{1-x}Be_xO$ can theoretically be tuned from 3.37 to 10.60 eV, this materials system may replace $Zn_{1-x}Mg_xO$ solid solutions which are being considered in applications such as polymer-oxide hybrid solar cells, field effect transistors, high- k

films on Si, quantum Hall effect devices, acoustic resonators and large electromechanical coupling [18–21].

The literature on $Zn_{1-x}Be_xO$ is limited to a few experimental and theoretical studies that concentrate on the electronic structure, band gap energies, and optical properties [15,16,22–25]. To the best of our knowledge, the phononic and thermodynamic properties of this alloy are less studied. The knowledge of phonon and thermodynamic properties of $Zn_{1-x}Be_xO$ alloy are required in the development of high quality optoelectronic devices. The potential applications of $Zn_{1-x}Be_xO$ alloy system for applications described above have not been fully explored. In this work, we examine the elastic, phononic and thermodynamic properties of the $Be_xZn_{1-x}O$ alloy by the first principle theoretical method.

The paper is organized as follows: in the next section we give a brief description of the computational details. In Section 3, the results and discussions of structural and elastic properties of $Zn_{1-x}Be_xO$ are studied. Then the phonon properties of the $Zn_{1-x}Be_xO$ including phonon dispersion relations and partial phonon densities of states (PDOS) are studied using the density functional perturbation theory (DFPT) method. Temperature dependence of thermal properties such as free energy, specific heat, enthalpy, entropy and Debye temperature are predicted in the last part. Finally, we present our conclusions.

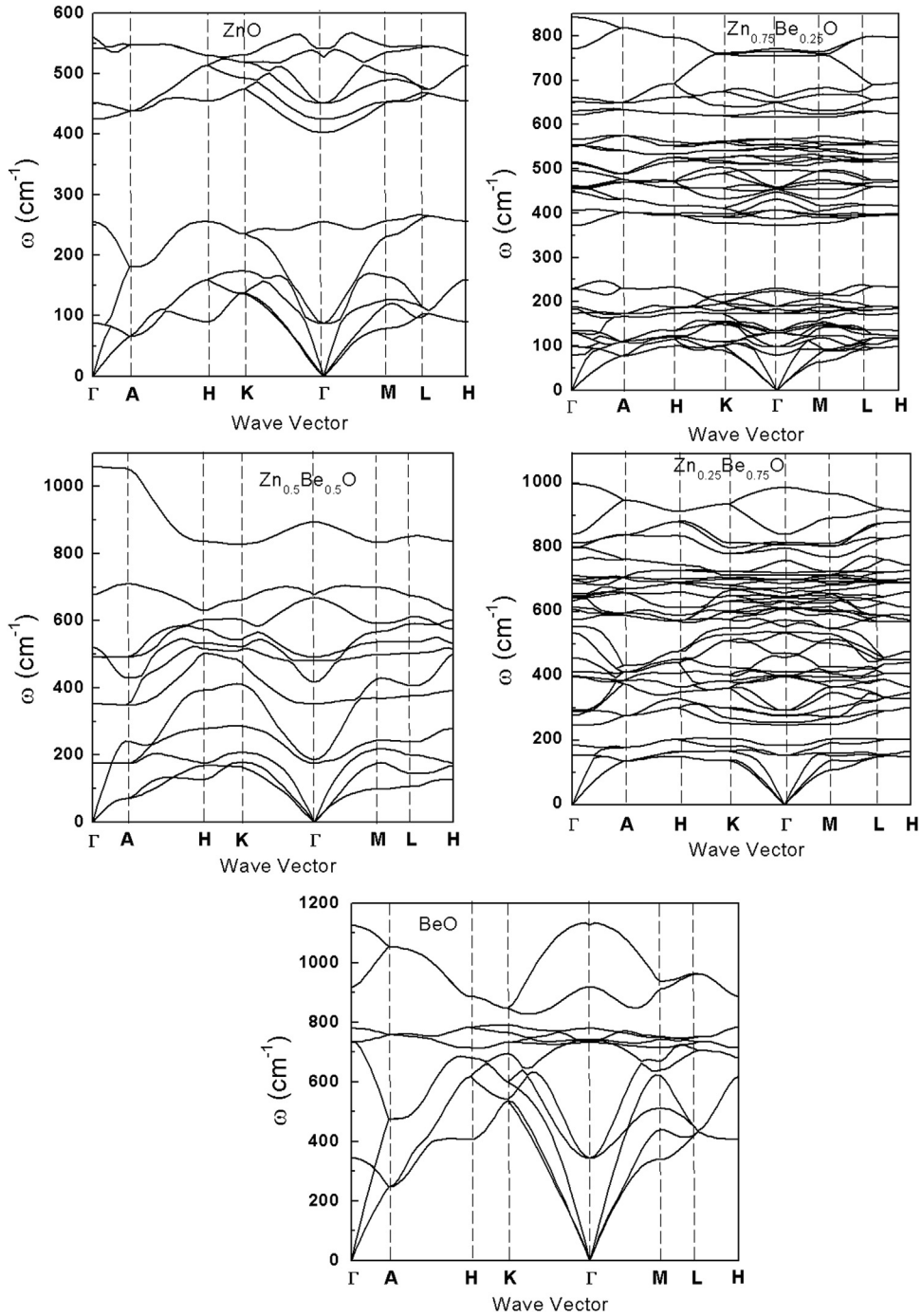


Fig. 1. Calculated phonon dispersion curves of $Zn_{1-x}Be_xO$ alloy for $x=0, 0.25, 0.5, 0.75$, and 1 along several high-symmetry lines in the BZ.

2. Computational methods

All the calculations are carried out using a plane wave pseudo potential method based on the density functional theory (DFT), implemented in the Cambridge Serial Total Energy Package (CASTEP) code. The exchange-correlation functional is treated within the PW91 generalized gradient approximation (GGA) [26]. The interaction between ion core and valence electrons is described by Norm-

conserving pseudopotential (NCP) [27]. Electronic states of Zn ($3d^{10} 4s^2$), O ($2s^2 2p^4$) and Be ($2s^2$) are treated as the valence-electron configuration for the zinc, oxygen and beryllium atoms, respectively, to describe the *electron-ion interaction*. According to the special quasi-random structures (SQS) approach [28], the $Zn_{1-x}Be_xO$ ($x=0.0, 0.25, 0.5, 0.75$, and 1.0) structures can be obtained by replacing 1–8 Zn atoms with Be in the $2 \times 2 \times 1$ wurtzite ZnO supercell. The convergence of the total energy with respect to both

Table 3Calculated optical phonon frequencies (in cm^{-1}) at the Γ point of the Brillouin zone for $\text{Zn}_{1-x}\text{Be}_x\text{O}$, compared to experimental data.

ZnO		$\text{Zn}_{0.75}\text{Be}_{0.25}\text{O}$		$\text{Zn}_{0.5}\text{Be}_{0.5}\text{O}$		$\text{Zn}_{0.25}\text{Be}_{0.75}\text{O}$		BeO	
Mode	Raman	Mode	Raman	Mode	Raman	Mode	Raman	Mode	Raman
E_2	92.85	E_2	98.24	E	175.91	E_2	153.33	E_2	336.92
	100 ^a	E_1	127.15	E	352.97	E_1	245.25		329.71 ^b
A_1	388.24	E_2	133.22	A_1	480.61	A_1	270.88		329.89 ^b
	380 ^a	E_1	171.17	E	491.21	E_2	292.58		337.3 ^c
	379 ^d	E_2	187.62	A_1	669.64	E_2	396.43	E_2	6.60
E_1	414.45	A_1	222.55	A_1	894.74	E_1	402.05		658.75 ^b
	410 ^a	E_1	368.56			E_1	412.17		720.6 ^b
	411 ^d	A_1	385.78			E_2	533.61		683 ^c
E_2	441.08	E_2	403.34			E_1	572.52	A_1	705.84
	438 ^a	E_2	452.84			E_2	606.27		658.89 ^b
	439 ^{d,e}	E_1	452.18			A_1	612.20		717.79 ^b
		E_2	510.23			E_2	630.88		678 ^c
		E_1	515.26			E_1	642.65	E_1	775.66
		A_1	540.58			A_1	645.49		699.5 ^b
		E_1	547.96			E_2	697.55		757.35 ^b
		E_2	562.66			E_1	713.96		722.7 ^c
		A_1	612.98			A_1	721.17		
		E_2	649.75			E_1	796.66		
		E_1	658.37			A_1	805.57		
		A_1	751.56			E_2	813.35		

^a Ref. [45].^b Ref. [48].^c Ref. [49].^d Ref. [46].^e Ref. [47].

k -point sampling and plane-wave cutoff energy is carefully examined. The plane-wave basis set with an energy cutoff 700 eV has been applied, and the $5 \times 5 \times 6$ Monkhorst-Pack mesh has been used for the Brillouin-zone (BZ) k -point sampling. Noting that, the structural optimizations were carried out using a Broyden–Fletcher–Goldfarb–Shanno (BFGS) minimization technique [29]. The tolerances for geometry optimization were set as the difference of total energy within 1.0×10^{-6} eV/atom.

The lattice dynamic properties are calculated on the corresponding optimized crystal geometries. The phonon frequencies are obtained as second-order derivatives of the total energy with respect to an external electric field or to atomic displacements within the framework of DFPT [30].

3. Results and discussion

3.1. Structural and elastic properties

First, we calculated the equilibrium structural parameters for the parent binary compound ZnO, in the wurtzite structure. There are 16 atoms 8 (Zn) and 8 (O) which correspond to a $2 \times 2 \times 1$ supercell. When we add the Be atom to the ZnO, in order to obtain $\text{Zn}_{1-x}\text{Be}_x\text{O}$, the alloys were modeled at some selected compositions $x=0.25, 0.5, 0.75$, and 1.

The calculated lattice constants for each x of the $\text{Zn}_{1-x}\text{Be}_x\text{O}$ alloys are summarized in Table 1, along with the other experimental and theoretical values available in the literature [31–33].

The present results agree well with the previous experimental [31,32] and theoretical [32,33] reports for the binary compounds ZnO and BeO.

In addition, the calculated structure parameters of $\text{Zn}_{0.75}\text{Be}_{0.25}\text{O}$, $\text{Zn}_{0.5}\text{Be}_{0.5}\text{O}$ and $\text{Zn}_{0.25}\text{Be}_{0.75}\text{O}$ are in agreement with theoretical work [33]. The results listed in Table 1 show that the lattice constants, a and c , decrease with increasing Be concentration. This phenomenon occurs because the atom radius of beryllium is smaller than that of zinc.

Elastic constants characterize the ability of the material to deform under any small stresses. They also determine the first order contribution to strain energy-content as the material is strained. The effect of strain on the physical properties is also important in terms of getting some knowledge of the nano-mechanical properties of the materials. Usually, elastic constants are defined by means of a Taylor expansion of the total energy $E(V, \delta)$ for the system with respect to a lattice strain δ of the primitive cell volume V . The energy of a strained system is expressed as follows [34]:

$$E(V, \delta) = E(V_0, 0) + V_0 \left(\sum_i \tau_i \xi_i \delta_i + \frac{1}{2} \sum_{ij} C_{ij} \delta_i \xi_i \delta_j \xi_j \right) \quad (1)$$

where $E(V_0, 0)$ is the energy of unstrained system with equilibrium volume V_0 , τ_i is an element in the stress tensor, ξ_i and ξ_j are factors to take care of Voigt index. There are five independent elastic constants for hexagonal structure, i.e., C_{11} , C_{33} , C_{44} , C_{12} , and C_{13} .

The mechanical stability conditions of the elastic constants in hexagonal crystal are known as to be [35,36] at 0 GPa

$$C_{11} > 0, C_{11} - C_{12} > 0, C_{44} > 0, (C_{11} + C_{12})C_{33} - 2C_{13}^2 > 0 \quad (2)$$

The computed elastic constants C_{11} , C_{12} , C_{13} , C_{33} and C_{44} for wurtzite $\text{Zn}_{1-x}\text{Be}_x\text{O}$ alloys are listed in Table 2. We notice that the values of elastic constants change continuously from those of ZnO to those of BeO as Be concentration increases

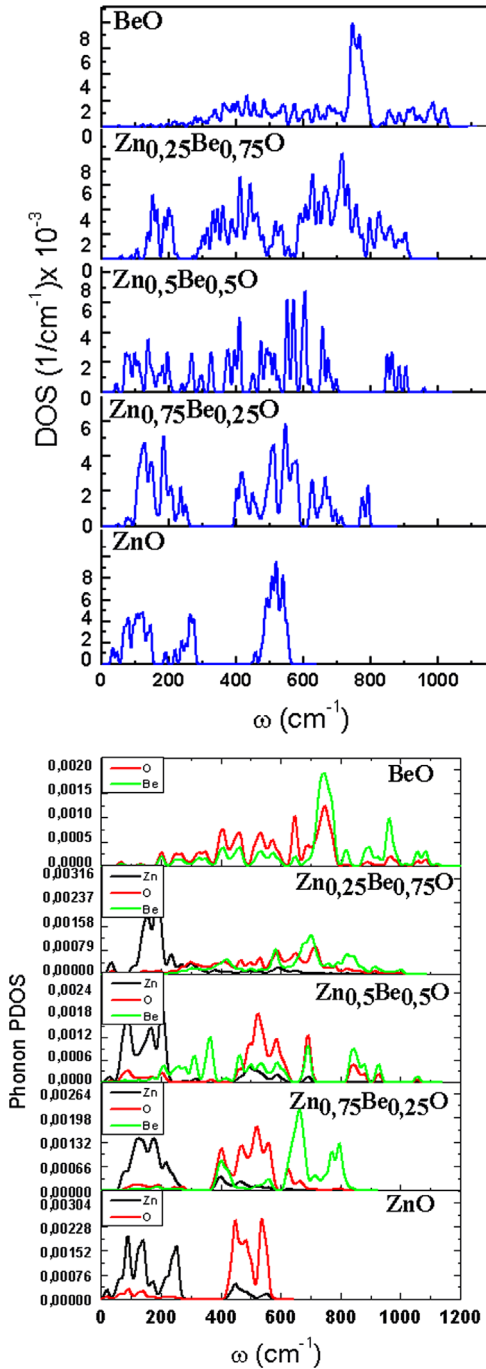


Fig. 2. The calculated density of states: (a) total phonon density of states (TDOS), and (b) partial densities of states (PDOS) for $Zn_{1-x}Be_xO$ alloy.

from 0% up to 100%, although the overall trend can be formulated as follows: in the entire range of concentration x , the elastic constants C_{11} , C_{33} and C_{44} increase with the increase of Be content, except for C_{12} and C_{13} which have slow decrease when Be concentration increases. Obviously, from the calculated values of C_{ij} in Table 2, the above restrictions are all satisfied, implying that $Zn_{1-x}Be_xO$ alloys as a function of Be concentration are mechanically stable.

3.2. Phonon spectrum and density of states (DOS)

The harmonic approximation is usually a typical description for the physics of phonon, in which the equation of motion takes the form of [43]

$$\omega^2(k, l)e(k, l) = D(k)e(k, l) \quad (3)$$

where $\omega(k, l)$ is the phonon frequencies, $e(k, l)$ describing the corresponding atomic displacement, k is the wave vector, l is the number of phonon branches, $l=1, 2, \dots, 3n$, is equal to the number of degree of freedom in the primitive unit cell, $D(k)$ is the dynamic matrix, which can be obtained from the force constant matrix Φ .

$$D_{st}^{\alpha\beta}(k) = \frac{1}{\sqrt{M_s M_t}} \sum_R \Phi_{st}^{\alpha\beta}(R) \exp(-ikR) \quad (4)$$

where M_s and M_t are masses of the atoms s and t , respectively, R is the Bravais lattice vectors. Within the frame work of harmonic approximation, keeping only the second terms in the Taylor series of total energy E , Φ is given by

$$\Phi_{st}^{\alpha\beta} = \frac{\partial^2 E}{\partial \mu_s^\alpha \partial \mu_t^\beta} \quad (5)$$

where μ_s^α is the displacement of atom s from its equilibrium position in α direction.

The phonon dispersion and partial phonon densities of states are calculated by using the linear-response method within the density functional perturbation theory DFPT [30].

The wurtzite modification of ZnO, BeO and $Zn_{0.5}Be_{0.5}O$ with the space group C_{6v} and C_{3v} , respectively, has $n=4$ atoms in the primitive unit cell which lead to $3n=12$ vibrational eigen modes (3 acoustical and 9 optical modes). Thus the vibration frequency at the Brillouin zone-center Γ point ($q=0$) is called as normal vibration mode. The standard group theory analysis yields the following decomposition of the optical vibrational representation in irreducible representation of group C_{6v} and C_{3v} , respectively, at Γ point as follows:

$$\Gamma_{Opt}^{ZnO} = 1 A_1^{(R+IR)} + 4 E_2^{(R)} + 2 E_1^{(R+IR)} + 2 B_2^{(S)}$$

where IR and R correspond to infrared and Raman active modes, respectively. Here, all modes except B_2 are active in Raman spectra, whereas only those with A_1 and E_1 symmetry are allowed in infrared spectra. Consequently, there are totally 3 infrared and Raman active modes, 4 Raman active modes and 2 silent (S) modes.

The calculated phonon dispersion relations along the high symmetry direction of the Brillouin zone (BZ) for $Zn_{1-x}Be_xO$ are shown in Fig. 1. No imaginary phonon frequency, i.e. negative frequencies, at any wave vectors, indicating the dynamical stabilities of $Zn_{1-x}Be_xO$ alloy.

Fig. 1 indicates clearly the shift up of the phonon energy with the increase of Be content. This shifting of the $Zn_{1-x}Be_xO$ is very obvious in both the optical phonon branches and the acoustic phonon branches. This is mainly caused by two reasons:

- 1 Stronger bond force in $Zn_{1-x}Be_xO$: according to the formalism described by Segall et al. [44], the calculation of bond population of Zn–O for $Zn_{0.75}Be_{0.25}O$ and Be–O for $Zn_{0.25}Be_{0.75}O$ are respectively 0.32 and 0.55.

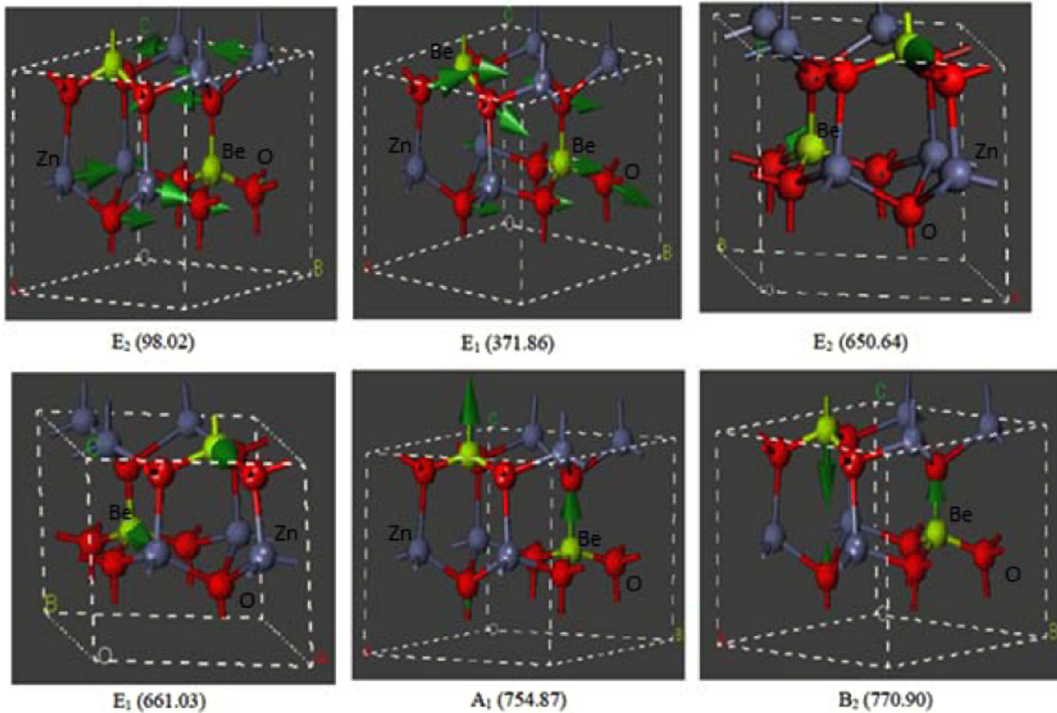


Fig. 3. Atomic displacement patterns of $\text{Zn}_{0.75}\text{Be}_{0.25}\text{O}$.

The smaller bond population between Zn–O than that between Be–O is indicative of a stronger Be–O bond than that of Zn–O bond. Stronger inter-atomic bonding force means higher phonon frequencies.

2 *Light atomic mass in $\text{Zn}_{1-x}\text{Be}_x\text{O}$* : the second reason is the different atomic masses between Zn and Be elements. The lighter mass of Be increases the vibration frequency. As a result, the phonon frequencies of ZnO ($x=0$) are lower than those of BeO ($x=1$) (see Fig. 1).

Table 3 presents the optical phonon frequencies calculated at Γ point for $\text{Zn}_{1-x}\text{Be}_x\text{O}$ corresponding to $x=0.0, 0.25, 0.50, 0.75$ and 1.0 , respectively. Unfortunately, there are no experimental data and theoretical values concerning $\text{Zn}_{0.75}\text{Be}_{0.25}\text{O}$, $\text{Zn}_{0.5}\text{Be}_{0.5}\text{O}$ and $\text{Zn}_{0.25}\text{Be}_{0.75}\text{O}$ for comparison, so our results are predictions, while the phonon frequencies obtained for ZnO and BeO are in good agreement with experimental and theoretical data in Refs. [44–48].

The partial phonon densities of states are displayed in Fig. 2 for better understanding of contributions to phonon structure of each atom. Generally, the low frequency modes below 300 cm^{-1} are mainly from Zn atom, and the high frequency modes (above 360 cm^{-1}) are dominated by the partial DOS of Be. The partial phonon DOS of $\text{Zn}_{1-x}\text{Be}_x\text{O}$ indicates clearly that Zn atoms contribute more to the low frequency region than Be and O atoms, because of the heavier mass of Zn than the other two atoms. It is interesting to note that there exists overlaps between optical phonons and acoustic phonons in a broad frequency for $\text{Zn}_{0.5}\text{Be}_{0.5}\text{O}$, $\text{Zn}_{0.25}\text{Be}_{0.75}\text{O}$ and BeO . This is

different in the case of $\text{Zn}_{0.75}\text{Be}_{0.25}\text{O}$ and ZnO , as there is a phonon band gap at frequency about 78.55 cm^{-1} and 125.45 cm^{-1} for $\text{Zn}_{0.75}\text{Be}_{0.25}\text{O}$ and ZnO , respectively. This can be understood from the atomic masses of O, Be and Zn, while the significantly large atomic mass of Zn results in the phonon band gap.

The vibration motions of low-frequency region ($\leq 300\text{ cm}^{-1}$) are mainly related to the translational movements of Zn and O atoms. The vibration motions of E_2 mode at 98.02 cm^{-1} translational movements of Zn and half of O atoms, and the Be and half of O atoms are kept still. In addition, the translational vibrations in the high-frequency region ($\geq 360\text{ cm}^{-1}$) are mainly related to the movements of Be and O atoms. For the E_1 mode at 375.86 cm^{-1} , the Be and O atoms have translational movements with each other along the y axis and half of Zn atoms move in the opposite direction along the y axis. It can be seen from Fig. 3 that at the E_2 mode (at 650.64 cm^{-1}) the Be atoms have translational motions move opposite each other along the y axes and half of O atoms move against each other along the y axis, while all Zn and half of O atoms keeping still. For the E_1 mode (at 661.03 cm^{-1}) involves the translational movements of Be and half of O atoms, Be atoms move in the opposite direction along the y axis and one half of O atoms move along the y axis, and the other half of O and all Zn atoms nearly are kept still. The A_1 mode (at 754.87 cm^{-1}) involves the translational movements of Be and half of O atoms. Be atoms move along the z axis with one half of O atoms move against each other along the z axis, and the other Zn and half of O atoms nearly are still. For the silent B_2 mode at 770.90 cm^{-1} , involves the translational movements half of O and Be atoms. The half of O

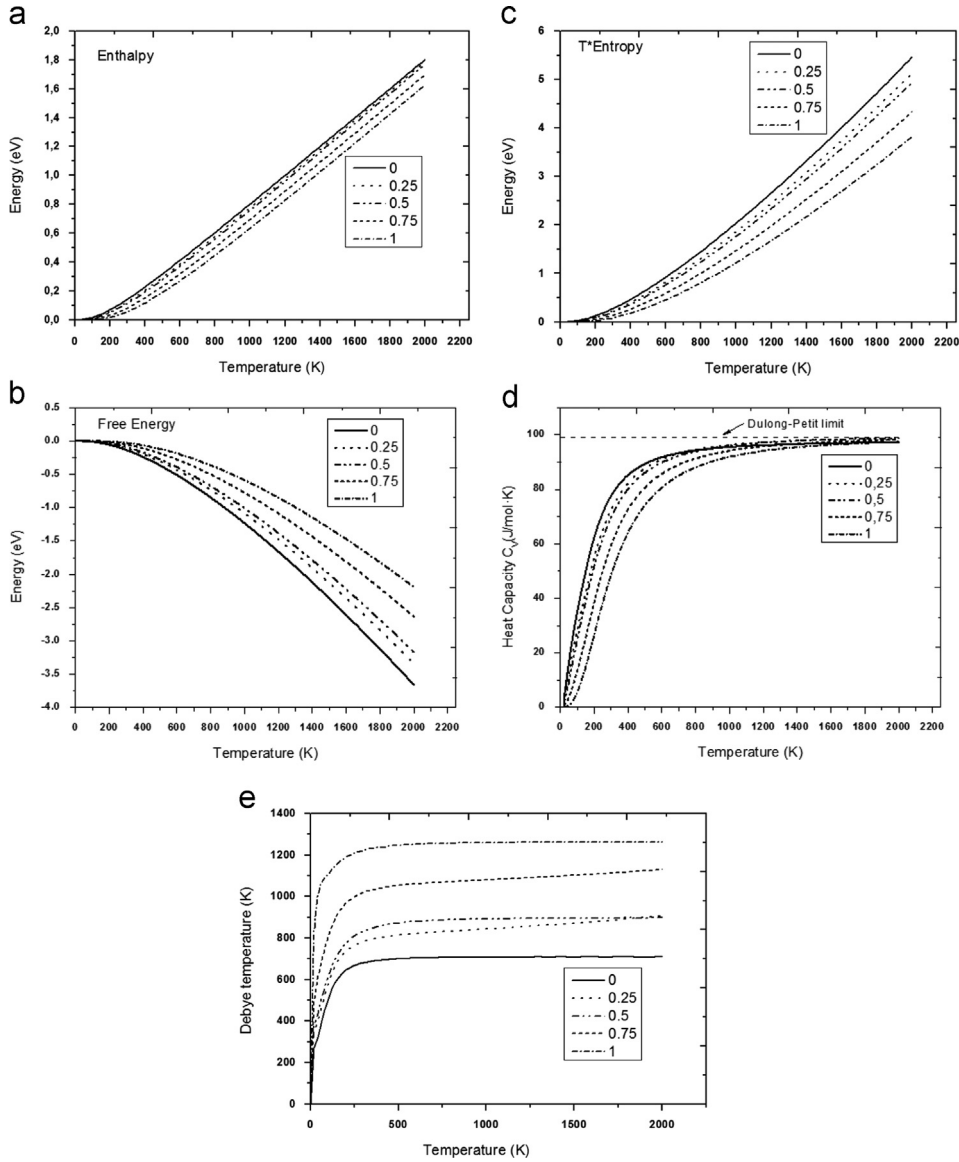


Fig. 4. The calculated thermodynamic properties for $\text{Zn}_{1-x}\text{Be}_x\text{O}$ in the temperature range of 0–2000 K, (a) enthalpy, (b) free energy, (c) T^* entropy, (d) heat capacity and (e) Debye temperature.

and Be atoms move against each other along the z axes, and the Zn and half of O atoms are still.

3.3. Temperature-dependent thermodynamic properties

The temperature-dependent thermodynamic properties of a crystal, such as the energy (E), entropy (S), free energy (F) and lattice heat capacity C_v , can be calculated from their phonon density of states as a function of frequencies [30]. The temperature dependence of the energy E can be obtained using

$$E(T) = E_{\text{tot}} + E_{\text{zp}} + \int \frac{\hbar\omega}{\exp(\hbar\omega/k_B T) - 1} g(\omega) d\omega \quad (6)$$

where E_{zp} is the zero point vibrational energy, k_B is the Boltzmann constant, \hbar is the Planck constant and $g(\omega)$ is

the phonon density of states. E_{zp} can be evaluated as

$$E_{\text{zp}} = 1/2 \int g(\omega) \hbar\omega d\omega \quad (7)$$

The vibrational contributions to the Helmholtz free energy F , the entropy S , the constant-volume heat capacity C_v and the constant-volume heat capacity in the Debye model C_v^D [50] are given by

$$F(T) = E_{\text{tot}} + E_{\text{zp}} + k_B T \int g(\omega) \ln[1 - \exp(-\hbar\omega/k_B T)] d\omega \quad (8)$$

$$S(T) = k_B \left\{ \int \frac{\hbar\omega/k_B T}{\exp(\hbar\omega/k_B T) - 1} g(\omega) d\omega - \int g(\omega) [1 - \exp(-\hbar\omega/k_B T)] d\omega \right\} \quad (9)$$

$$C_v(T) = k_B \int \frac{(\hbar\omega/k_B T)^2 \exp(\hbar\omega/k_B T)}{[\exp(\hbar\omega/k_B T) - 1]^2} g(\omega) d\omega \quad (10)$$

$$C_v^D(T) = 9Nk_B \left(\frac{T}{\theta_D}\right)^3 \int \frac{x^4 e^x}{(e^x - 1)^2} dx \quad (11)$$

where N is the number of atoms per cell, and θ_D is the Debye temperature at a given temperature T . By fitting the theoretical C_v^D , the temperature dependence of θ_D can be obtained.

The temperature dependence of Helmholtz free energy, vibration entropy, enthalpy, specific heat C_v and Debye temperature θ_D for $\text{Zn}_{1-x}\text{Be}_x\text{O}$ solid solutions in range 0–2000 K are shown in Fig. 4. From Fig. 4(a)–(c), below 82 K, the values of the enthalpy, entropy and free energy for $\text{Zn}_{1-x}\text{Be}_x\text{O}$ are almost zero. Above 82 K, the free energy decreases gradually with increasing temperature. However, when temperature increases, the calculated entropy and enthalpy increase continually. The free energy is higher for larger x . This suggests that a solid solution with lower Be content is thermodynamically more stable. From Fig. 4(a)–(c), the entropy and the enthalpy decrease with the increase in beryllium composition.

In Fig. 4(d) and (e), we presented the results of the temperature dependences of the heat capacity at constant volume C_v and Debye temperature θ_D for wurtzite $\text{Zn}_{1-x}\text{Be}_x\text{O}$. In the low temperature limit, the C_v exhibits the T^3 power-law behavior, and they all approach at high temperature, the specific heat approaches to the Dulong–Petit limit $C_v = 3nk_B N_A = 99.2 \text{ J/mol K}$, with $n=4$ is the number of atoms in primitive cell and N_A is the Avogadro's number. At room temperature, the heat capacities are 77.72, 72.61, 69.67, 59.33 and 48.27 J/mol K with the increasing x , respectively. It is known that for solids the difference between C_p and C_v is negligible at low temperatures, our calculated value of C_v is smaller than the experimental data of $C_p=40.45 \text{ J/mol K}$ in [51] for ZnO, while, our calculated value of C_v for BeO is in fairly good agreement with the experimental C_v values and 40.18 J/mol K in [52] at room temperature.

The Debye temperature is a suitable parameter to describe phenomena of solid state physics which are associated with lattice vibration, elastic constants, specific heat and melting point. The calculated Debye temperature is shown in Fig. 4(e). The θ_D increases rapidly below 250 K and reaches a maximum of 709.66, 908.43, 898.27, 1130.21 and 1262.76 K for $\text{Zn}_{1-x}\text{Be}_x\text{O}$ corresponding to $x=0.0, 0.25, 0.50, 0.75$ and 1.0, respectively. The Debye temperature θ_D was measured to be 416 K for ZnO [53] and to be 1270 K for BeO [54], showing an excellent agreement with our calculated values. There is no experimental or theoretical data concerning the heat capacities and the Debye temperature for $\text{Zn}_{0.75}\text{Be}_{0.25}\text{O}$, $\text{Zn}_{0.5}\text{Be}_{0.5}\text{O}$ and $\text{Zn}_{0.25}\text{Be}_{0.75}\text{O}$, respectively, where our results are predictions.

4. Conclusion

In this paper, a fundamental analysis of the elastic, phononic and thermodynamic properties of $\text{Zn}_{1-x}\text{Be}_x\text{O}$ alloy has been performed using DFT and DFPT calculations. The calculated equilibrium lattice parameters and elastic constants are in good agreement with experimental and theoretical data. Phonon dispersion relations show that

acoustic and optic phonon branches shift to higher frequencies with the increase of Be content, which is due to the difference between atomic mass (m_{Zn} and m_{Be}) and strong Be–O bond. Calculated phonon dispersions show that $\text{Zn}_{1-x}\text{Be}_x\text{O}$ are dynamically stable. The phonon dispersion curves, phonon density of states are also calculated. Zone center phonon frequencies are in good agreement with experimental Raman spectra. The values of the heat capacity C_v and the Debye temperature θ_D change as Be concentration increases from 0 to 100%. While, our results are in reasonable agreement with the experimental data and theoretical values for ZnO and BeO. Finally, the free energy increases with the increasing Be concentration, while the enthalpy and entropy gradually decrease with the increasing Be content. Free energy calculations indicate that $\text{Zn}_{1-x}\text{Be}_x\text{O}$ is thermodynamically more stable with lower Be content.

References

- [1] Z.P. Wei, Y.M. Lu, D.Z. Shen, Z.Z. Zhang, B. Yao, B.H. Li, J.Y. Zhang, D.X. Zhao, X.W. Fan, Z.K. Tang, *J. Korean Phys. Soc.* 53 (2008) 3038–3042.
- [2] Y.D. Ko, K.C. Kim, Y.S. Kim, *Superlattice Microstruct.* 51 (2012) 933–941.
- [3] D. Karanth, H. Fu, *Phys. Rev. B* 72 (2005) 064116.
- [4] A. Tubtimtae, M.W. Lee, *Superlattice Microstruct.* 52 (2012) 987–996.
- [5] E.M.C. Fortunato, P.M.C. Barquinha, A.C.M.B.G. Pimentel, A.M. F. Goncalves, A.J.S. Marques, L.M.N. Pereira, R.F.P. Martins, *Adv. Mater.* 17 (2005) 590–594.
- [6] J.-H. Lim, C.-K. Kang, K.-K. Kim, I.-K. Park, D.-K. Hwang, S.-J. Park, *Adv. Mater.* 18 (2006) 2720–2724.
- [7] D.K. Hwang, S.H. Kang, J.H. Lim, E.J. Yang, Y.J. Oh, J.H. Yang, S.J. Park, *Appl. Phys. Lett.* 86 (2005) 222101–222103.
- [8] Y.R. Ryu, T.S. Lee, H.W. White, *Appl. Phys. Lett.* 83 (2003) 87–89.
- [9] T. Yamada, T. Nebiki, S. Kishimoto, H. Makino, K. Awai, T. Narusawa, T. Yamamoto, *Superlattice Microstruct.* 42 (2007) 68–73.
- [10] S. Venkatachalam, Y. Iida, Y. Kanno, *Superlattice Microstruct.* 44 (2008) 127–135.
- [11] C. Klingshirn, *Phys. Status Solidi* 244 (2007) 3027–3073.
- [12] H.D. Sun, T. Makino, Y. Segawa, M. Kawasaki, A. Ohtomo, K. Tamura, H. Koinuma, *J. Appl. Phys.* 91 (2002) 1993–1997.
- [13] M.J. Vellekoop, C.C.O. Visser, P.M. Sarro, A. Venema, *Sens. Actuators A: Phys.* 23 (1990) 1027–1030.
- [14] T. Makino, Y. Segawa, M. Kawasaki, A. Ohtomo, R. Shiroki, K. Tamura, T. Yasuda, H. Koinuma, *Appl. Phys. Lett.* 78 (2001) 1237–1239.
- [15] Y.R. Ryu, T.S. Lee, J.A. Lubguban, A.B. Corman, H.W. White, J.H. Leem, M.S. Han, Y.S. Park, C.J. Youn, W.J. Kim, *Appl. Phys. Lett.* 88 (2006) 052103–052105.
- [16] X.F. Fan, Z. Zhu, Y.S. Ong, Y.M. Lu, Z.X. Shen, J.L. Kuo, *Appl. Phys. Lett.* 91 (2007) 121121–121123.
- [17] Y.R. Ryu, T.S. Lee, H.W. White, *J. Cryst. Growth* 261 (2004) 502–507.
- [18] M. Nakano, A. Tsukazaki, A. Ohtomo, K. Ueno, S. Akasaka, H. Yuji, K. Nakahara, T. Fukumura, M. Kawasaki, *Adv. Mater.* 22 (2010) 876–879.
- [19] D.C. Olson, S.E. Shaheen, M.S. White, W.J. Mitchell, M.F.A.M. van Hest, R.T. Collins, D.S. Ginley, *Adv. Funct. Mater.* 17 (2007) 264–269.
- [20] A. Tsukazaki, S. Akasaka, K. Nakahara, Y. Ohno, H. Ohno, D. Maryenko, A. Ohtomo, M. Kawasaki, *Nat. Mater.* 9 (2010) 889–893.
- [21] Y. Chen, P. Reyes, Z. Duan, G. Saraf, R. Wittstruck, Y. Lu, O. Taratula, E. Galoppini, *J. Electron. Mater.* 38 (2009) 1605–1611.
- [22] T.S. Jeong, M.S. Han, J.H. Kim, S.J. Bae, C.J. Youn, *J. Phys. D* 40 (2007) 370–373.
- [23] J.M. Khoshman, D.C. Ingram, M.E. Kordes, *Appl. Phys. Lett.* 92 (2008) 091902–091903.
- [24] S.F. Ding, G.H. Fan, S.T. Li, K. Chen, B. Xiao, *Physica B* 394 (2007) 127–131.
- [25] H.L. Shi, Y. Duan, *Eur. Phys. J. B* 66 (2008) 439–444.
- [26] J.P. Perdew, J.A. Chevary, S.H. Vosko, K.A. Jackson, M.R. Pederson, D. J. Singh, C. Fiolhais, *Phys. Rev. B* 46 (1992) 6671–6687.
- [27] D.R. Hamann, M. Schluter, C. Chiang, *Phys. Rev. Lett.* 43 (1979) 1494–1497.

- [28] A. Zunger, S.H. Wei, L.G. Ferreira, J.E. Bernard., *Phys. Rev. Lett.* 65 (1990) 353–356.
- [29] B.G. Pfrommer, M. Côté, S.G. Louie, M.L. Cohen, J. *Comp. Physiol.* 131 (1997) 133–140.
- [30] S. Baroni, S. de Gironcoli, A.D. Corso, P. Giannozzi, *Rev. Mod. Phys.* 73 (2001) 515–562.
- [31] F. Decremps, F. Datchi, A.M. Saitta, A. Polian, S. Pascarelli, A.D. Cicco, J.P. Itie, F. Baudelet, *Phys. Rev. B* 68 (2003) 104101–104104.
- [32] A. Schleife, F. Fuchs, J. Furthmüller, F. Bechstedt, *Phys. Rev. B* 73 (2006) 245212.
- [33] Zheng Yongping, Chen Zhigao, Lu Yu, Wu Qingyun, Weng Zhenzhen, Huang Zhigao, *J. Semicond.* 29 (12) (2008) 2316–2321.
- [34] L. Fast, J.M. Wills, B. Johansson, O. Eriksson, *Phys. Rev. B* 51 (1995) 17431–17438.
- [35] M. Born, K. Huang, *Dynamical Theory of Crystal Lattices*, Oxford University Press, London, 1954.
- [36] M.S. Islam, A.K.M.A Islam, *Physica B* 406 (2011) 275–279.
- [37] G. Carloti, D. Fioretto, G. Socino, E. Verona, *J. Phys. Condens. Matter* 7 (1995) 9147.
- [38] S. Saib, N. Bouarissa, *Phys. Status Solidi (b)* 244 (2007) 1063–1069.
- [39] P. Gopal, N.A. Spalpin, *J. Electron. Mater.* 35 (2006) 538–542.
- [40] Yifeng Duan, Hongliang Shi, Lixia Qin, *Phys. Lett. A* 372 (2008) 2930–2933.
- [41] F. Wang, J. Wu, C. Xia, C. Hu, P. Zhou, L. Shi, Y. Ji, Z. Zheng, X. Liu, *J. Alloy. Compd.* 597 (2014) 50–57.
- [42] *Semiconductors: Data Handbook*, in: O. Madelung (Ed.), third ed. Springer, Berlin, 2004.
- [43] E. Kaxiras, *Atomic and Electronic Structure of Solids*, Cambridge University Press, New York, 2003.
- [44] M.D. Segall, C.J. Pickard, R. Shah, M.C. Payne, *Population analysis in plane wave electronic structure calculations* *Mol. Phys.* 89 (1996) 571–577.
- [45] J. Serrano, A.H. Romero, F.J. Manjón, R. Lauck, M. Cardona, A. Rubio, *Phys. Rev. B* 69 (2004) 094306–094319.
- [46] F.J. Manjón, K. Syassen, R. Lauck, *High Press. Res.* 22 (2002) 299–304.
- [47] F. Decremps, J. Pellicer-Porres, A.M. Saitta, J.-C. Chervin, A. Polian, *Phys. Rev. B* 65 (2002) 092101–092105.
- [48] Fen Luo, Yan Cheng, Ling-Cang Cai, Xiang-Rong Chen, *J. Appl. Phys.* (2013) 033517-1–033517-8.
- [49] A. Bosak, K. Schmalzl, M. Krisch, W. Van Beek, V. Kolobanov, *Phys. Rev. B* 77 (2008) 224303–224310.
- [50] N.W. Ashcroft, N.D. Mermin, *Solid State Physics*, Saunders College, Philadelphia, 1976.
- [51] *Gmelin Handbuch, Anorg. Chem.* 32 (1956) 803.
- [52] B.E. Walker Jr., C.T. Ewing, R.R. Miller., *J. Chem. Eng.* 7 (1962) 595–597.
- [53] R.A. Robie, J.L. Edwards, *J. Appl. Phys.* 37 (1966) 2659–2663.
- [54] O.L. Anderson, *J. Phys. Chem. Solids* 24 (1963) 909–917.